

Article

# Principal Subspace of Dynamic Functional Connectivity for Diagnosis of Autism Spectrum Disorder

Mohammed Isam Al-Hiyali <sup>1</sup>, Norashikin Yahya <sup>1,\*</sup>, Ibrahima Faye <sup>1</sup>, Maged S. Al-Quraishi <sup>1</sup>  
and Abdulhakim Al-Ezzi <sup>2</sup>

<sup>1</sup> Centre for Intelligent Signal and Imaging Research (CISIR), Department of Electrical and Electronic Engineering, Universiti Teknologi PETRONAS, Seri Iskandar 32610, Perak, Malaysia

<sup>2</sup> Neurosciences, Huntington Medical Research Institutes, Pasadena, CA 91105, USA

\* Correspondence: norashikin\_yahya@utp.edu.my; Tel.: +60-53687861

**Abstract:** The study of functional connectivity (FC) of the brain using resting-state functional magnetic resonance imaging (rs-fMRI) has gained traction for uncovering FC patterns related to autism spectrum disorder (ASD). It is believed that the neurodynamic components of neuroimaging data enhance the measurement of the FC of brain nodes. Hence, methods based on linear correlations of rs-fMRI may not accurately represent the FC patterns of brain nodes in ASD patients. In this study, we proposed a new biomarker for ASD detection based on wavelet coherence and singular value decomposition. In essence, the proposed method provides a novel feature-vector based on extraction of the principal component of the neuronal dynamic FC patterns of rs-fMRI BOLD signals. The method, known as principal wavelet coherence (PWC), is implemented by applying singular value decomposition (SVD) on wavelet coherence (WC) and extracting the first principal component. ASD biomarkers are selected by analyzing the relationship between ASD severity scores and the amplitude of wavelet coherence fluctuation (WCF). The experimental rs-fMRI dataset is obtained from the publicly available Autism Brain Image Data Exchange (ABIDE), and includes 505 ASD patients and 530 normal control subjects. The data are randomly divided into 90% for training and cross-validation and the remaining 10% unseen data used for testing the performance of the trained network. With 95.2% accuracy on the ABIDE database, our ASD classification technique has better performance than previous methods. The results of this study illustrate the potential of PWC in representing FC dynamics between brain nodes and opens up possibilities for its clinical application in diagnosis of other neuropsychiatric disorders.

**Keywords:** autism spectrum disorder; resting state fMRI; BOLD signal; dynamic functional connectivity; SVD; principal component; oriented energy



**Citation:** Al-Hiyali, M.I.; Yahya, N.; Faye, I.; Al-Quraishi, M.S.; Al-Ezzi, A. Principal Subspace of Dynamic Functional Connectivity for Diagnosis of Autism Spectrum Disorder. *Appl. Sci.* **2022**, *12*, 9339. <https://doi.org/10.3390/app12189339>

Academic Editor: Keun Ho Ryu

Received: 24 August 2022

Accepted: 14 September 2022

Published: 18 September 2022

**Publisher's Note:** MDPI stays neutral with regard to jurisdictional claims in published maps and institutional affiliations.



**Copyright:** © 2022 by the authors. Licensee MDPI, Basel, Switzerland. This article is an open access article distributed under the terms and conditions of the Creative Commons Attribution (CC BY) license (<https://creativecommons.org/licenses/by/4.0/>).

## 1. Introduction

Autism spectrum disorder (ASD) is a group of neurodevelopmental disorders characterized by difficulties in social interactions, language delay, and repetitive behaviors. The World Health Organization (WHO) reports that ASD affects 1 in 160 children worldwide [1]. Moreover, the severe deficits associated with ASD place a significant health and financial burden on the global community [2]. Given the increasing prevalence of ASD, it is important to further develop ASD diagnostic tools to reduce the impact of this burdens and to better manage ASD subjects. In the Diagnostic and Statistical Manual of Mental Disorders (DSM), the American Psychological Association (APA) has classified ASD into three subtypes based on impairment symptoms: classic autistic disorder (ASD), Asperger syndrome (APD) and pervasive developmental disorder—not otherwise specified (PDD-NOS) [3]. The different impairment ratings for ASD subtypes are based on repetitive behaviors, verbal skills, social interaction and communication. Diagnosis of autism is a difficult task because there is no standard medical test for accurate diagnosis [4]. Current clinical practice uses

various questionnaires based on cognitive characteristics and behavioral observations for diagnosis of ASD [5–8]. The disadvantages of these clinical assessments, which require direct interaction between the child and the clinician, are that they are time-consuming and costly. Because symptom-based diagnostic criteria depend on observational techniques and subjective decisions, autism researchers point out that diagnoses of ASD types vary widely from clinic to clinic, even when they are all based on the same standard tests [8]. Because clinical results are imprecise, there is a need to find accurate biological markers to automate the ASD diagnostic process [9]. Automated solutions based on artificial intelligence (AI) can enable rapid ASD classification, hence increasing the reliability and accuracy of diagnostic results [10,11]. Experts have recently developed many AI algorithms for ASD diagnostic models based on functional magnetic resonance imaging (fMRI). Previous works have shown that resting-state functional magnetic resonance imaging (rs-fMRI) data play an essential role in diagnosing ASD. Because rs-fMRI has better spatial resolution, it enables the functional analysis of deep brain structures [11]. In particular, rs-fMRI is commonly used to study functional connectivity (FC) of the brain at rest by detecting fluctuations in blood oxygenation-dependent (BOLD) signals. Essentially, FC identifies the spatio-temporal correlations between brain regions based on BOLD signals [12]. The different patterns of FC in ASD are mainly used with AI algorithms to create ASD classifiers that distinguish ASD from normal cases (NC) [13–15].

## 2. Related Work

In the last 10 years, rs-fMRI techniques have been used in the study of brain activity for diagnosis of ASD using machine learning and deep learning algorithms [16–18]. Table A1 in the Appendix A presents the latest AI technologies in ASD classification using rs-fMRI data from the Autism Brain Imaging Data Exchange (ABIDE). As shown in Table A1, support vectors machines (SVMs) are a traditional machine learning classifier that has been widely used in previous studies. Chen et al. [19] proposed a discriminative model using an SVM to classify the selected FC features based on the F-score method. With 240 ASD and 128 NC subjects, the data were collected from six different sites of ABIDE, producing 79.17% classification accuracy based on 10-fold cross validation (CV). Bernas et al. [20] also used SVM for classification of ASD, taking in-phase synchronization features of the FC network extracted from 30 subjects from one of the ABIDE sites: the LEUVEN dataset. Their classification technique achieved an average accuracy of 86.7% using 30-fold CV. Recently, Ma et al. [21] extracted the phase synchrony of the FC network and used principal component analysis (PCA) to reduce the dimensionality of the FC network by selecting the best FC features as the feature vector for the SVM classifier. Using a dataset of 90 subjects, the classifier achieved 78.9% accuracy in ASD classification from NC run on a 10-fold CV framework.

As shown above, the selection of discriminative FC features in fMRI data is crucial for good performance of discriminative models for ASD detection. On the other hand, deep learning (DL) algorithms based on FC networks of rs-fMRI data have been used to classify ASD. Heinsfeld et al. [16] concluded that DL algorithms should use unsupervised methods to extract relevant features while minimizing human intervention. They transferred 19,900 features from the FC network to a deep neural network (DNN) using two stacked denoising auto-encoders and achieved an average accuracy of 70%. Wang et al. [22] achieved 93.2% accuracy by using SVM with recursive feature elimination (RFE) to select the top-ranked FC features from an FC network; their results were based on 10-fold CV among the full ABIDE dataset. Sherkatghanad et al. [17] attempted to improve the automated ASD classifier by converting the vector of FC features to two-dimensional (2D) matrices and using the images as input to a convolutional neural network (CNN). Their proposed model achieved an average accuracy of 70.2% based on 10-fold CV. In the same context, Hunag et al. [18] achieved 76.4% average classification accuracy using 2D images of selected FC features as input to a deep belief network (DBN). Huang et al. [18] first filtered the FC network using a heuristic graph-based feature selection method that considered

both external and internal FC network measurements. Subah et al. [23] achieved 87.9% ASD classification accuracy by training a DNN using the FC features of rs-fMRI data from ABIDE. Based on the quality assessment of the fMRI data, the authors selected 866 patients from a total number of 1035, including 402 ASD and 464 NC subjects.

It is worth mentioning that the brain network pattern FC plays a key role in the performance of ASD classification models. As can be seen from Table A1, there are two main patterns of FC: static and dynamic. To determine the static FC network, the Pearson correlation between the BOLD signals of the brain nodes is used. Most studies that have used rs-fMRI data to classify ASD utilized static FC [16–18]. On the other hand, dynamic connections can be obtained by representing the FC in the time–frequency domain, resulting in more informative connectivity features.

For example, Chen et al. [19] examined the resting-state FC in ASD over two frequency bands: the slow-4 (0.01–0.027 Hz) and slow-5 (0.027–0.073 Hz). Bernas et al. [20] attempted to study FC networks based on in-phase synchronization of coherence between signals, and Ma et al. [21] determined the dynamic correlation between brain nodes based on phase synchrony coefficients. Exciting new work has shown that viewing the brain FC as dynamic over time and frequency can successfully reveal the disruptions of the normal human brain in a disordered state [24,25].

At present, the accuracy of ASD classification models based on multiple ABIDE training datasets ranges from 70–93% over the full ABIDE database. However, despite the increasing number of automated classification models, it remains a challenge to find discriminative models that provide superior accuracy with low false prediction in FC-based ASD diagnosis. Clearly, inaccurate predictions can have a negative impact on a patient's life and even cause financial costs for healthcare institutions [26,27]. For example, if a model misclassifies an ASD patient as a normal case or misidentifies ASD subtypes, the disorder may go untreated and may worsen the patient's impairment symptoms. In this case, there can be serious consequences for the reputation and performance of health facilities.

On the premise of ensuring a robust and efficient ASD diagnostic model, this study proposes a new dynamic FC as an ASD biomarker for more accurate classification of ASD from NC. Evidence suggests that the temporal dynamics of FC is a key feature in identifying brain disorders [20,21].

Therefore, we proposed a new metric called wavelet coherence fluctuations (WCF), which represents the amplitude of coherence between brain regions during low-frequency fluctuations using the wavelet coherence transform. The functional brain network is constructed based on WCF, and biological ASD markers are identified by using a variance analysis-support vector machine (ANOVA-SVM) method. Then, the wavelet coherence plus singular value decomposition is implemented to generate a 2D matrix representing the coherence of the ASD biomarkers based on the pure time–frequency components. This matrix is known as the principal wavelet coherence (PWC) connectivity. By using SVD, the useful properties of the WC matrix in classifying ASD vs. NC can be extracted. Then, the PWC matrix is converted into a 2D image. Finally, a three-layer CNN (3L-CNN) is used as an AI algorithm to examine the performance of the proposed framework in identifying ASD patients using PWC images.

Three main sections of the paper are presented as follows: the methodology in Section 3 explains the complete ASD classification methods based on the principal subspace of dynamic functional connectivity, including the WCF calculation, the ANOVA-SVM algorithm, the PWC generation and the proposed CNN models. Section 4 presents the results and discussion, and lastly, Section 5 provides the conclusion and future works.

### 3. Material and Method

The overall methodology in developing ASD classification using the ASD FC patterns of rs-fMRI data is shown in Figure 1. The rs-fMRI data preparation, FC measurements, identification of ASD FC patterns, 2D FC image construction and classification networks are illustrated in the following sections.

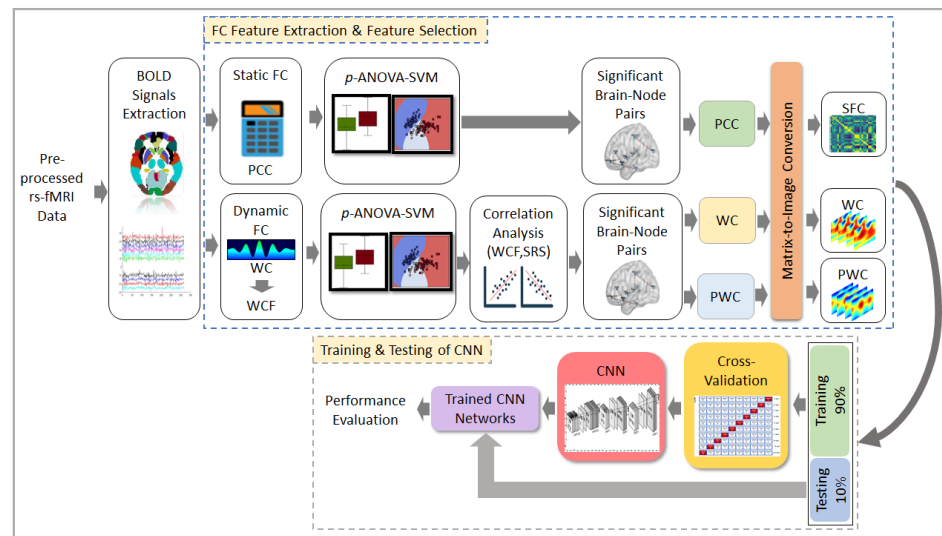


**Figure 1.** Method of investigation in the development of automatic ASD diagnosis using PWC of resting-state fMRI BOLD signals and convolutional neural networks.

### 3.1. rs-fMRI Data Preparation

First, preprocessed ABIDE rs-fMRI data are downloaded from the Preprocessed Connectomes Project (PCP) database, and the Data Processing Assistant for rs-fMRI (DPARSF) is selected [28]. The ABIDE data include 1035 subjects collected from different universities and institutions, of which 505 are ASD subjects and 530 are NC subjects. Details about the dataset, its scanning parameters and the number of subjects are listed in Table 1.

**Table 1.** Details of rs-fMRI ABIDE database for ASD and NC subjects acquired using 3T MRI scanner.

Site	Country	Manufacturer	Time Points ( $TP_t$ )	# of ASD	# of NC	Total
SDSU	US	GE	175	14	22	36
STANFORD	US	GE	235	19	20	39
UM	US	GE	295	66	74	140
KKI	US	Philips	151	20	28	48
LEUVEN-1	Belgium	Philips	245	14	15	29
LEUVEN-2	Belgium	Philips	245	15	19	34
SBL	Netherlands	Philips	195	15	15	30
TRINITY	Ireland	Philips	145	22	25	47
CALTECH	US	Siemens	145	19	18	37
CMU	US	Siemens	315	14	13	27
MAX	Germany	Siemens	115	24	28	52
NYU	US	Siemens	175	75	100	175
OHSU	US	Siemens	77	12	14	26
OLIN	US	Siemens	215	19	15	34
PITT	US	Siemens	195	29	27	56
UCLA	US	Siemens	115	54	44	98
USM	US	Siemens	235	46	25	71
YALE	US	Siemens	195	28	28	56
Overall	-	-	-	505	530	1035

Legend: SDSU, San Diego State University; STANFORD, Stanford University; UM, University of Michigan; KKI, Kennedy Krieger Institute; LEUVEN, University of Leuven; SBL, Social Brain Lab; Trinity, Trinity College Institute of Neuroscience; CALTECH, California Institute of Technology; CMU, Carnegie Mellon University; MAX, Ludwig Maximilian University of Munich; NYU, New York University; OHSU, Oregon Health and Science University; OLIN, Olin Center; Institute of Living at Hartford Hospital; PITT, University of Pittsburgh School of Medicine; UCLA, University of California; Los Angeles; USM, University of Utah School of Medicine; Yale, Yale School of Medicine.

For extraction of BOLD signals, Automated Anatomical Labeling (AAL) is chosen as the default brain atlas; it essentially divides the brain into 90 nodes [29]. For each subject, the BOLD signal is extracted at each brain node, and this forms a matrix  $B \in \mathbb{R}^{TP_t \times \text{node}}$ , where each column contains the BOLD signal of length  $TP_t$  of a specific node =  $[1, 2, \dots, 90]$ .

### 3.2. Functional Connectivity (FC) of BOLD Time-Series Signals

Functional connectivity of fMRI signals provides a measure of correlation or similarity between brain nodes and is commonly used in discriminating various neurological disorders [24,30,31]. The calculation of FC from fMRI is obtained from BOLD time-series signals extracted for specific brain nodes according to the type of brain atlas. The conventional method of FC is based on Pearson correlation coefficients (PCCs) and are classified as a type of static FC since it is based only on the time-domain information. On the other hand, FC based on wavelet coherence (WC) is a dynamic FC due to the fact that the wavelet transform provides time–frequency resolution of 1D signals. The decomposition into time–frequency localization of wavelet-based FC essentially provides additional information for better discrimination of neurological disorders [20,32]. In the subsequent sections, the theory of static and dynamic FC is provided in detail.

#### 3.2.1. Static FC Using Pearson Correlation Coefficients (PCC)

For static FC (SFC), the use of Pearson correlation coefficients (PCCs) of BOLD signals is a common linear method for determining functional connectivity between different areas of the brain and provides useful information about brain activity [17,18]. Calculating the PCC between two BOLD signals involves finding their covariance (cov) and dividing by the product of their standard deviations. If  $x(t)$  and  $y(t)$  represent the BOLD signals of two nodes, the PCC of the two nodes is

$$\beta_{x,y} = \frac{\text{cov}(x,y)}{\sigma_x \sigma_y}, \quad (1)$$

where for  $x(t)$  and  $y(t)$ , the standard deviation is represented by  $\sigma_x$  and  $\sigma_y$ , respectively. By subtracting the mean value of the BOLD signals and determining the expected value, the covariance can be calculated as follows

$$\text{cov}(x,y) = E[(x - \mu_x)(y - \mu_y)], \quad (2)$$

where  $E[.]$  denotes the expected value, and  $\mu_x$  and  $\mu_y$  denote the mean of  $x(t)$  and  $y(t)$ , respectively.

#### 3.2.2. Dynamic FC Using Wavelet Coherence (WC)

For dynamic FC (DFC), wavelet coherence (WC) is a nonlinear estimator used to determine functional connectivity between brain areas using time–frequency components of neuroimaging signals [20,32]. Based on the Grinsted et al. [33] method, the WC can be calculated by first extracting the time–frequency components from each BOLD signal using the continuous wavelet transform (CWT). As given in Equation (3), the CWT coefficient is defined as the convolution of the BOLD signal  $x(t)$  with the scaled and translated form of a mother wavelet  $\psi_{a,b}(t)$ .

$$\text{CWT}(a,b) = \frac{1}{\sqrt{a}} \int_{-\infty}^{\infty} x(t) \psi^* \left( \frac{t-b}{a} \right) dt, \quad (3)$$

where  $a$  is the wavelet scale,  $b$  is the location, and  $*$  indicates the complex conjugate [34]. The Morlet wavelet is used as the mother wavelet because it has the best ratio (1.03) between frequency band and wavelet scale, which facilitates the understanding of data in the frequency domain [35]. CWT is emerging as an important method in biosignal analysis due to its ability to extract useful information from non-stationary signals [36,37]. Further, WC, which is based on CWT, characterizes coherence measures between two signals on different time scales and does not require assumptions about the stationarity of the input signals. As a result, CWT provides a good balance between time and frequency components.

The next step is to calculate the joint power of the BOLD signal pair  $x, y$  at different scales  $a$  and times  $b$  using the following equation

$$C_{xy}(a,b) = S(C_x^*(a,b)C_y(a,b)), \quad (4)$$

where  $C_x(a, b)$  and  $C_y(a, b)$  respectively denote the CWT of  $x$  and  $y$  at scales  $a$  and positions  $b$ , the superscript  $*$  is the complex conjugate, and  $S$  is smoothing in time and scale. Then, the WC between  $x$  and  $y$  is calculated by

$$WC_{xy} = \frac{|C_{xy}(a, b)|^2}{(S|C_x(a, b)|^2)(S|C_y(a, b)|^2)} \tag{5}$$

The WC is a 2D matrix,  $WC \in \mathbb{R}^{TP_t \times F}$ , and the matrix coefficient is denoted as  $wc_{t,f}$ , where  $t = 1, 2, \dots, TP_t$  is the number of time points, and  $f = 1, 2, \dots, F$  is the number of frequency scales based on wavelet decomposition at low frequency fluctuation (LFF) (0.01–0.08 Hz). The matrix represents the time–frequency components of the coherence between pairs of BOLD signals, with each row reflecting the coherence of a particular pair of brain nodes  $x$  and  $y$  across time  $t$ . The column of the WC matrix represents 37 frequency bands spaced equally from 0.01 Hz to 0.08 Hz; hence  $F = 37$ . The values of time points  $TP_t$  for each rs-fMRI dataset are listed in Table 1.

For example, Figure 2 illustrates the 145-length BOLD signal pairs selected from a subject of the CALTECH dataset. As can be seen in Figure 2, the coherence values of the signal pairs range between 0 and 1. These values indicate the similarity between  $x(t)$  and  $y(t)$  at different phases. As defined by Grinsted et al. [33], the phase difference in wavelet coherence is from  $x(t)$  over  $y(t)$  at scales  $a$  and positions  $b$  is

$$\phi_{xy} = \tan^{-1} \frac{\Re(C_{xy}(a, b))}{\Im(C_{xy}(a, b))} \tag{6}$$

where  $\Re(C_{xy}(a, b))$  is the real part, and  $\Im(C_{xy}(a, b))$  is the imaginary part of  $C_{xy}(a, b)$ . A phase difference of zero means that there is no coherence between the signals. When  $\phi_{xy} \in (0, \frac{\pi}{2})$ , the BOLD signals are coherently in-phase, with the first signal  $x(t)$  lagging the second signal,  $y(t)$ , whereas when  $\phi_{xy} \in (-\frac{\pi}{2}, 0)$ ,  $x(t)$  leads  $y(t)$ . When  $\phi_{xy} \in (-\pi, -\frac{\pi}{2})$ , the BOLD signals are in anti-phase with  $x(t)$  lagging  $y(t)$ , and when  $\phi_{xy} \in (\frac{\pi}{2}, \pi)$ ,  $x(t)$  leads  $y(t)$ . The arrows in Figure 2 indicate this behavior of the phase differences between the signals.

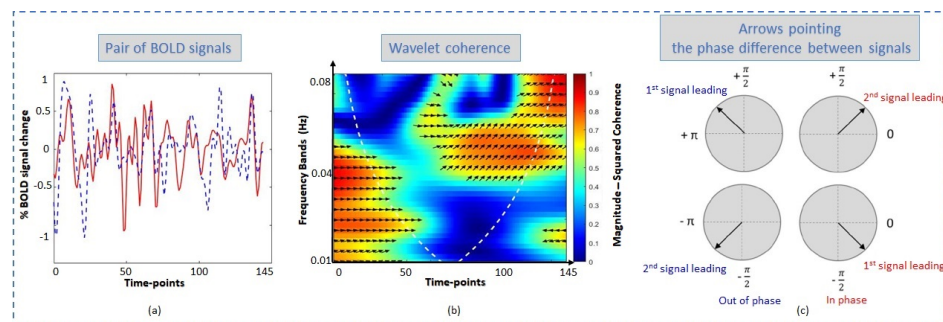


**Figure 2.** Wavelet coherence formation of (a) a pair of BOLD signals, (b) its corresponding wavelet coherence and (c) arrows showing the phase difference between the two signals  $x(t)$  and  $y(t)$ . The vertical and horizontal axes in (b) show the frequency and recording time of the BOLD signals, respectively. In (b), the darker red regions represent a higher degree of coherence, and the white overlay defines the cone of influence. In (c), the arrows are indications of the phase coherence, which is the ratio of leading to lagging signal.

### 3.3. Selection of the Most Significant ASD-Related Functional Connectivity

When scaling the analysis to multiple subjects and brain regions, the huge amount of information that a WC analysis generates presents a challenge, since a WC matrix is generated for each pair of BOLD signals. In this case, it is necessary to select the best brain-node pairs or FCs for classification of autism, thereby reducing the computational cost as well as improving the performance of the classifier.

To achieve this goal, we propose the framework illustrated in Figure 3. In essence, with 90 brain-region nodes, the method takes in 4005 values for the WC matrix and computes the wavelet coherence fluctuations (WCF), followed by ANOVA-SVM evaluation and lastly correlation analysis. From ANOVA-SVM, a subset of the most significant FCs is selected, and this subset is further reduced using the correlation analysis between the WCF of the selected FC with the Social Responsiveness Scale (SRS) score. In the subsequent sections, detailed description of the steps involved in selecting the most significant FCs for ASD are given.

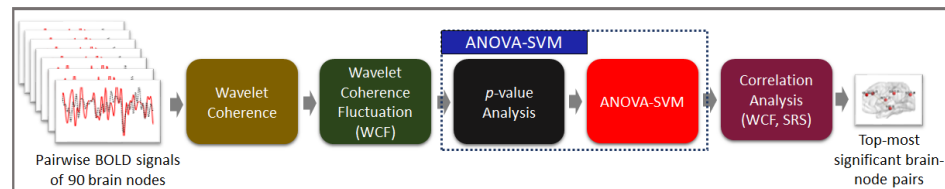


**Figure 3.** Method of selecting the most significant brain-node pairs from wavelet coherence using WCF, ANOVA-SVM and correlation analysis between WCF and SRS.

### 3.3.1. Wavelet Coherence Fluctuation (WCF) Measure

Prior to applying the  $p$ -ANOVA-SVM for each subject, the 4005-value WC matrix is transformed to a 1D matrix with a length of 4005. This 2D-to-1D matrix conversion is achieved by our newly proposed metric called wavelet coherence fluctuation (WCF). WCF estimates the total coherence variability in the low-frequency fluctuations of the BOLD signals. To determine the WCF, first the average (AV) of the wavelet coherence coefficients (rows of the WC matrix) at each frequency band over the time points is determined as follows

$$AV_{wc_t} = \frac{1}{TP_t} \sum_{t=1}^{TP_t} wc_t \quad (7)$$

Then, the averaged coefficients are summed over a given frequency scale as follows

$$WCF_{x,y} = \frac{1}{F} \sum_{f=1}^F AV_{wc_t} \quad (8)$$

Most rs-fMRI studies [19,38] have used the low frequency range of 0.01–0.08 Hz, relying on the results established in [13]. In addition, Biswal et al. [13] discovered that BOLD signals in the LFF contain physiologically significant information that can be used to analyze neural processes in a variety of brain disorders.

### 3.3.2. ANOVA-SVM and Correlation Analysis

In the first step to find the most discriminative FC related to ASD, the ANOVA-SVM algorithm is applied to the WCF feature vector. The size of the WCF matrix is the total number of subjects  $\times$  4005. ANOVA-SVM is a supervised learning algorithm that uses a heuristic search strategy to identify which of the 4005 connectivity features significantly contribute to the identification of ASD-FC patterns. A detailed description of the ANOVA-SVM steps can be found in Algorithm 1. Here, the  $p$ -value is the threshold used to control the size of subsets of FC. In our experiment, five subsets were determined by setting the  $p$ -value in the range (0.01:0.01:0.05). Then, each subset of the FC network is evaluated in terms of 10-fold CV classification accuracy by using the SVM classifier. The top subset of ASD FC is selected based on the highest classification scores for input to the correlation analysis stage. After that, correlation analysis is applied between the top subset of the FC network and the SRS scores to determine the significant connectivity features that correlate positively and negatively with ASD symptoms.

---

**Algorithm 1** ANOVA-SVM method for finding the top subset of connectivity features for discriminating ASD and NC

---

Input = Functional connectivity features vector

Output = ASD functional connectivity patterns

**initialization:**

$FC$  = Features vector for ASD and NC

producing  $4005 \times$  subject numbers per group

$F = \emptyset$  Subset of  $FC$

$B = \emptyset$  Index of top  $F$ -subset

1. **for**  $i = 1$  to 4005 **do**  
     ANOVA ( $FC(i)$ )  
      $p = p$ -value  
     **end**
  2. **While**  $0.01 \leq p \leq 0.05$  **do**  
      $F = FC(p)$ , where  $F \subset FC$   
     Classify  $F$  using SVM with 10-fold CV  
     Record the classification accuracy for each  $F$ -subset  
      $B =$  Index the  $F$ -subset with the highest classification accuracy  
     **end**
- 

Previous studies have shown that correlation analysis between FC features and clinical symptoms of ASD is helpful in discovering discriminative FC patterns for ASD patients [21,39,40]. In this study, correlation analysis between DFC measured using the WCF and clinical symptoms scores is conducted to find the subset of most significant FCs related to ASD. Clinical symptoms are represented by the Social Responsiveness Scale (SRS), with details given in Table 2 (Appendix A). The SRS is a tool used to assess the severity of autism symptoms. It consists of 65 items divided into five content-areas of social deficits: awareness (AWA), cognition (COG), communication (COM), motivation (MOT) and mannerism (MAN) [41].

**Table 2.** Demographic and mean value  $\pm$  standard deviation (SD) of clinical diagnostic SRS scores of LEUVEN dataset.

	ASD Mean (SD)	NC Mean (SD)	F-Test	$p$ -Value
No. of subjects	29 (26M/3F)	33 (28M/5F)	-	-
Age (years)	17.7 (0.9)	18.3 (0.8)	0.9	0.5
SRS_AWA	7.8 (0.6)	7.4 (0.8)	0.4	0.02
SRS_COG	10.2 (1.1)	10.4 (1.6)	0.4	0.00
SRS_COM	18.6 (1.7)	16.7 (2.8)	0.3	0.00
SRS_MOT	10.9 (1.1)	10.4 (1.5)	0.4	0.01
SRS_MAN	9.7 (1.0)	8.6 (1.4)	0.5	0.02
SRS_TOT	56.8 (4.9)	53.6 (7.8)	0.3	0.00

It should be noted that by using PCC, each subject will generate a single  $90 \times 90$  PCC matrix. The size of the 2D matrix generated by PCC is relatively small compared to the WC analysis. Therefore, the PCC undergoes only ANOVA-SVM. In addition, by comparing the accuracy results of PCC and WC from ANOVA-SVM, as covered in Table 3, it is clear that the WC method is superior to PCC. Hence, correlation analysis with SRS is not applied to PCC but only to WCF.

**Table 3.** Number of significant FC patterns of WCF and PCC based on classification accuracy (%) evaluated for 10-fold CV at different  $p$ -values (0.01–0.05) using ANOVA-SVM algorithm.

$p$ -Value	WCF		PCC	
	FC <sub>s</sub>	AccU	FC <sub>s</sub>	AccU
0.01	51	91.1 ± 0.3	47	90.3 ± 0.6
0.02	93	93.2 ± 0.2	87	91.8 ± 0.4
0.03	119	92.1 ± 0.2	131	86.5 ± 0.8
0.04	179	91.9 ± 0.1	168	82.7 ± 0.9
0.05	212	93.7 ± 0.3	204	87.6 ± 0.4

### 3.4. Principal Components of Wavelet Coherence

To further improve the classification of ASD using 2D matrices of WC analysis, we applied singular value decomposition (SVD) to extract the significant coherent components from the WC matrix [42]. This technique is known as principal wavelet coherence (PWC) and is illustrated in Figure 4. SVD basically decomposed the WC matrix into three matrices:  $U$ ,  $S$  and  $V$  as follows

$$WC_{(TP_t \times F)} = U_{(TP_t \times TP_t)} \cdot S_{(TP_t \times F)} \cdot V_{(F \times F)}^T \tag{9}$$

Here, the semi-unitary matrices  $U$  and  $V$  are real orthogonal matrices, and matrix  $S$  is real pseudo diagonal elements with non-negative diagonal entries. The measure  $S$  is used to determine when a single or a particular group of SVD components is dominant in the WC matrix. The diagonal entries  $S$  are called the singular values of the original WC matrix and are arranged in decreasing order. The  $u_i$  and  $v_i$  columns of  $U$  and  $V$  are called the left-singular and right-singular vectors of the matrix, respectively. The  $s_i$  values are ordered so that the one with the highest magnitude has the smallest index  $i$ . It is assumed that most of the coherence values of the SVD matrices are contained in the first principal component of the SVD. Hence, the output of the PWC stage is WC matrices reconstructed using first principal components. This means that apart from the first singular value, the rest of the singular values are set to zero. PWC is based on the development of our previous method for identifying ASD based on WC of rs-fMRI BOLD signals [32].

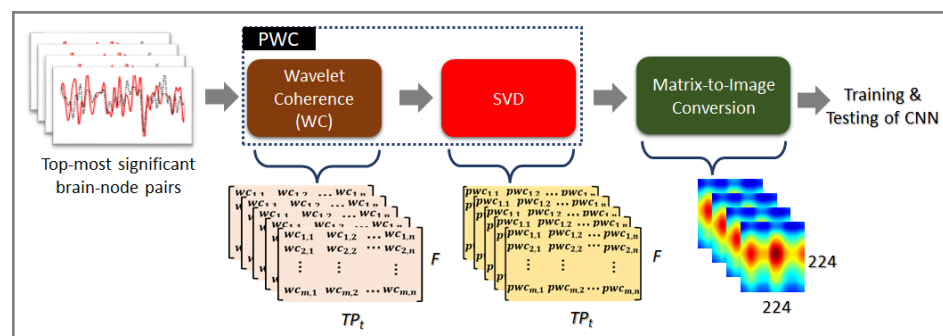


**Figure 4.** The formation of principal wavelet coherence (PWC) images as the input feature for training and testing of CNN. Here,  $TP_t$  indicates the length of the BOLD signals, and  $F$  is the number of frequency bands from 0.01 Hz to 0.08 Hz.

In the next step, the FC matrices based on SFC and DFC are separately converted into 2D images of size  $224 \times 224$  to be used as input to CNN for ASD classification. A total of 90% of the images per each type are used for training and validation, and the remaining 10% are used for blind testing. The steps to prepare the images for ASD classification are shown in Figure 4.

### 3.5. Classification Using CNN

Convolutional neural networks (CNNs) are one of the most important deep neural networks; they use local convolutional filters to extract regional image information [43,44]. In this study, we propose a three-layer CNN (3L-CNN) architecture, as shown in Figure 5 for ASD classification based on FC images. The proposed 3L-CNN consists of three convolutional blocks (ConLs) with filter size of  $7 \times 7$ . The ConLs blocks are connected to batch normalization (BanoL) to speed up training by reducing the internal shift of covariance within the network. In addition, these layers improve training speed while reducing the possibility of overfitting. Then, the rectifier function (ReLU) is implemented to determine whether the information contained in a BanoL node is useful, and based on this, it will decide whether the neural node should be activated or deactivated. After that, a max pooling layer (MPL) is applied to extract the maximum value of the rectified BanoL nodes. The output of the last MPL layer is then fed into the fully connected layer (FCL). The FCL output is set for binary classification to distinguish between ASD and NC by using a softmax layer.

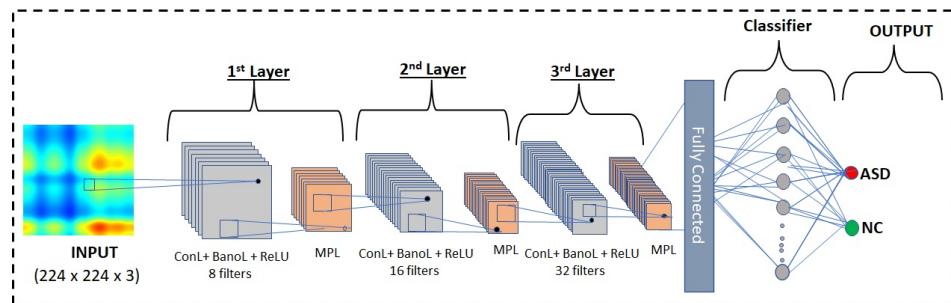


**Figure 5.** Structure of 3L-CNN for ASD diagnosis using FC-images of BOLD rs-fMRI signals.

### 3.6. ASD Diagnosis and Performance Evaluation

To practically evaluate the performance of our proposed CNN models, we compute the metrics given in Equations (10)–(13). Here, the True Positives (TPs) are the ASD patients that are correctly identified by the classifier, while False Negatives (FNs) are the normal cases (NC) that are incorrectly classified as positive. On the other hand, True Negatives (TNs) are negative images that are correctly classified as negative. In contrast, False Positives (FPs) are predictions that are incorrectly classified as positive.

$$\text{Accuracy (AccU)} = \frac{TP + TN}{TN + FN + FP + TP} \quad (10)$$

$$\text{Sensitivity (SenS)} = \frac{TP}{FN + TP} \quad (11)$$

$$\text{Specificity (SpeC)} = \frac{TN}{FP + TN} \quad (12)$$

$$\text{Precision (PreC)} = \frac{TP}{FP + TP} \quad (13)$$

In general, AccU in classification problems is the total number of correctly predicted ASD and NC subjects versus the total observed data. SenS measures the effectiveness of the proposed models in correct identification of the WC images of ASD, and SpeC measures the effectiveness of the models in identifying WC images of NC. Moreover, the receiver operating characteristic curve (ROC) and the area under curve (AUC) are also used for better visualization of the performance of a binary classifier. The ROC is a representation of sensitivity to specificity, and the AUC shows how well a method makes positive and negative categorical distinctions. A larger AUC is better and indicates the model's ability to distinguish between ASD and NC.

## 4. Results and Discussion

This section evaluates the performance of the proposed methods in identifying important FC patterns in classifying autism. Comparisons are made with the basic approach of previous studies using Pearson's correlation connectivity. In selecting the significant FCs, evaluation using ANOVA-SVM and subsequent correlation analyses are conducted using the LEUVEN dataset, which comes with the SRS scores. After selection of the most significant FCs, the proposed ASD classification framework is evaluated experimentally using 1035 subjects of the ABIDE dataset. Comparison is made between classifications based on three types of 2D image inputs: (1) DFC patterns using WC, (2) DFC patterns using PWC and (3) SFC patterns using PCC.

### 4.1. Identification of Top FC Features Using ANOVA-SVM Algorithm

For DFC, the connectivity of 90 regions generates 4005 images for each subject based on WC. This is a relatively large number of images compared to the number of subjects in each class. Selecting the best FCs from the 4005 values not only improves the training time of the CNN, but also improves classification performance. Further, the large number of images complicates the ability of the CNN models to correctly perform the classification task. For SFC, using all 4005 PCC scores may have a negative impact on classification performance. Therefore, the ANOVA-SVM algorithm is used to reduce the size of FC patterns based on the WCF and PCC scores. In addition, we hypothesized that the significant correlation between FCs and SRS scores provides better identification of neuronal biomarkers of ASD. Since only the LEUVEN dataset provides SRS scores, these subjects are used for this experiment. LEUVEN participants were recruited by a multidisciplinary team that included a psychiatrist and a neurologist who used the SRS tool to meet DSM criteria. Table 2 shows the details of the dataset and the SRS scores of the two groups as well as the results of the ANOVA tests showing significant differences ( $p$ -value  $\leq 0.05$ ).

The ANOVA-SVM algorithm is used to select the best subset of WCF and PCC features based on SVM accuracy, as shown in Section 3.3.2. Table 3 shows the average classification accuracy of each subset of connections using 10-fold CV. Table 3 shows that the SVM accuracy based on WCF ranges from 91.1% to 93.7% and based on PCC scores ranges from 87.6% to 91.8%. On the other hand, the variance of the accuracy values is lower for the WCF method than for the PCC method based on the standard deviations. According to these findings, WCF outperformed PCC in identifying ASD connectivity. This could be due to the fact that WCF better represents the neural activity of the brain, as WCF scores are determined using WC, which is a multivariate estimator. WCF is determined by averaging the correlation between two BOLD signals in the time–frequency domain, while PCC is evaluated in the time domain. Further, WCF overcomes the challenges mentioned by [24,25] in scaling analysis of the extensive information generated by WC. Compared to other DFC studies [19–21], the WCF metric is useful in providing information about the lag or lead of coherence between signals from multiple subjects and brain regions based on time–frequency analysis.

The improved representation of brain neural activity by WCF is useful for identifying neural biomarkers of ASD, which can be shown by correlation analysis with SRS scores in the next section. The high classification accuracy shown in Table 3 suggests that the severity of ASD symptoms is reflected by 212 brain connectivity functions. However, to determine which of these connections should be considered neural biomarkers for ASD, correlation analysis is performed between the WCFs of 212 connections and the ASD symptom scores of the SRS tool.

### 4.2. Correlation Analysis between WCF and SRS Scores

In this section, using the 212 FCs obtained using the ANOVA-SVM algorithm as described in the previous section, correlation analysis between WCF of the 212 FCs and SRS is conducted. This allows us to select the most important brain connections from the 212 connections that are more indicative of being ASD biomarkers. The results of the

correlation analysis are given in Table A2. Clearly, out of 212 connections, 35 connections are highly correlated with ASD symptoms. The criteria for selecting highly correlated pairwise WCFs are high correlation at >95% confidence level and SRS scores higher than four. Accordingly, there are five pairwise positive correlations and six pairwise negative correlations with ASD symptoms, as given in Table A2 in the Appendix A.

Plots of the main connections that positively and negatively correlate with SRS scores in the left and right hemispheres and all four lobes of the brain are shown in Figure 6a,b, respectively. These include the frontal lobe (MFG, SFGmed, SFGdor, ORBsup and ROL), the parietal lobe (SPG, PCUN and SMG), the occipital lobe (SOG and CAL) and the temporal lobe (STG, TPOmid, THA, HIP and OLF). For further validation, we compare the selected connections with the results of previous neuroscience studies [45–47]. It is noteworthy that the abnormality in FCs between MFG-HIP and THA-TPOmid is consistent with the results of [45,46]. In addition, Wy et al. [47] confirmed the presence of abnormalities in the functional connectivity of regions in the parietal lobe that correlate with performance of social skills of ASD subjects. According to these results, the selected autistic neural patterns based on WCF analysis can be used as biomarkers to better understand the dynamic neural mechanisms of ASD.

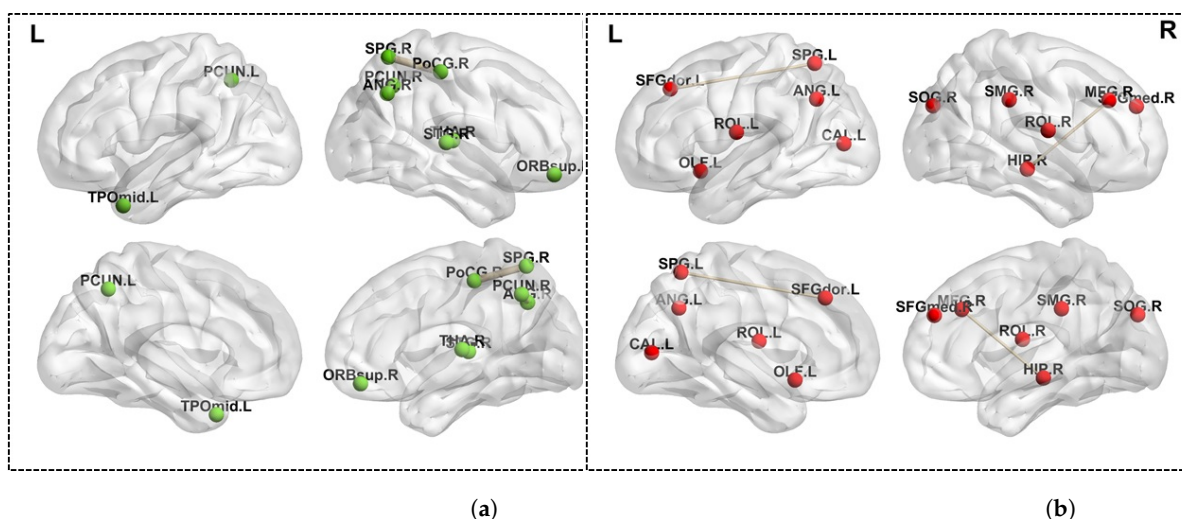


**Figure 6.** Brain nodes with (a) positive and (b) negative correlation with autism severity symptoms (SRS score) as listed in Table A2.

#### 4.3. Classification Evaluation Using PWC Matrices Reconstructed by Increasing Number of Principal Components

In this section, we present the results of an experiment to verify that the first principal component of a WC matrix is the one that carries the most important feature and provides the best classification accuracy. The FC matrix from the PWC block as illustrated in Figure 4 is WC, but it is reconstructed using only the first component, as in Equation (9). The performance of the 3L-CNN using WCs reconstructed using the first principal component through the first ten principal components is given in Figure 7.

It can be seen in Figure 7 that the classification accuracy decreases significantly as the number of principal components increases. It is clear that the first principal subspace, spanned by the first, leftmost eigenvector, senses the maximal oriented energy of the images, a concept that was highly discussed in [48]. It is then expected that the first principal component yields better accuracy than subsets with more than one of the leftmost eigenvectors. This trend is clearly evident from the plot of accuracy vs. number of principal components, i.e., the number of the leftmost eigenvectors, as shown in Figure 7.

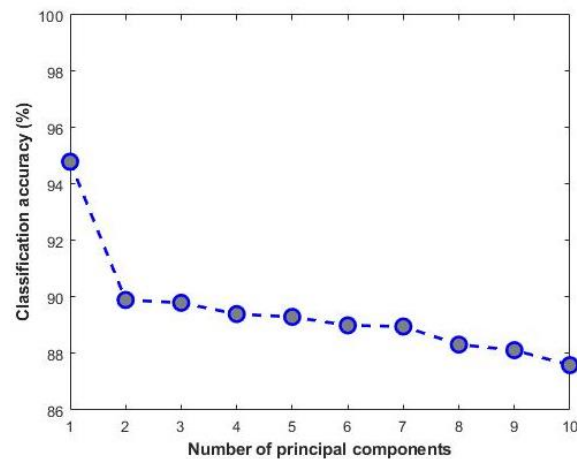


**Figure 7.** Classification accuracy (%) of 3L-CNN using PWC images reconstructed using first principal component through the first ten principal components. When using WC without application of SVD as input to the CNN, the classification accuracy of the 3L-CNN is 86.6%, as listed in Table 4.

**Table 4.** Percentage of average AccU, SenS, SpeC and PreC ( $\pm$ standard deviation) of the 3L-CNN using SFC, WC and PWC images based on 10-fold CV framework.

Metric	SFC	WC	PWC
AccU	72.3 $\pm$ 0.9	86.6 $\pm$ 1.6	95.2 $\pm$ 1.7
SenS	72.4 $\pm$ 1.3	84.8 $\pm$ 1.9	96.7 $\pm$ 2.4
SpeC	73.2 $\pm$ 1.1	88.4 $\pm$ 1.8	94.3 $\pm$ 4.5
PreC	72.8 $\pm$ 1.1	85.4 $\pm$ 1.3	94.8 $\pm$ 3.7

#### 4.4. Classification of ASD Using PWC FC Images

In this experiment, we evaluate the performance of FC images generated from DFC patterns, plus SFC patterns separately for ASD classification using CNNs. It is important to highlight that the full ABIDE dataset is a combination from 17 sites, giving a total of 505 ASD subjects and 530 NC subjects. The 3L-CNNs are trained using 90% of the data, consisting of 454 ASDs and 477 NCs under the framework of 10-fold CV, whereas, the test dataset comprising the remaining 10% of the data contains 51 ASD subjects and 53 NC subjects. The test data (10%) are considered outside the training dataset to validate generalization of the trained classifier model on unseen data. Here, the CNN models play the role of feature extraction and classification of the FC images and are able to capture high-ranking time–frequency features of WC and PWC images, as well as the features of SFC images.

For the DFC patterns, i.e., WC and PWC, 11 images of size  $224 \times 224 \times 3$  are generated from each subject for the BOLD signals of the node pairs listed in Table A2. The total number of FC images for training are 4994 for ASD and 5247 for NC. At the same time, 561 ASD images and 583 NC images are generated for the test dataset. Comparison is made with the conventional method of previous studies by using SFC images as input for the CNN [17,18]. The best PCC matrix has 87 significant connections out of a total of 90, as identified by the ANOVA-SVM algorithm and listed in Table 3. As input to the 3L-CNN, the PCC matrices are converted to 2D images of size  $224 \times 224 \times 3$ . Furthermore, the proposed CNN models are trained and tested on a computer equipped with an Nvidia GeForce RTX 2060 SUPER GPU. The model parameters were set as  $7 \times 7$  CNN filter size, batch size of 8 and ADAM optimizer based on the experimental results tabulated in Table A3 in the Appendix B.

##### 4.4.1. Evaluation of PWC-Based ASD Classification Using 10-Fold Cross Validation

In this section, we evaluate the performance of SFC, WC and PWC images for ASD classification. Essentially, this experiment is about observing the impact of PWCs on

classification performance. Table 4 shows the results of ASD classification of SFC, WC and PWC images using our proposed 3L-CNN model in terms of accuracy, sensitivity, specificity and precision using a 10-fold CV framework. From Table 4, classification using images from PWC outperforms images from SFC and WC, with the best average accuracy, sensitivity and specificity of 95.2%, 96.7% and 94.3%, respectively. ASD classification using PWC images was 8.6% and 22.9% higher than the WC and SFC images, respectively, based on 10-fold CV. The model performance based on the images from WC achieved 86.6% accuracy, which is a good result compared to the SFC images' 72.3% accuracy. However, it is worth noting that the use of SFC images achieves marginal improvement compared to previously published outcomes [18].

In addition, Figure 8 shows the ROC curve for the 3L-CNN model using SFC, WC and PWC images, indicating the value of the AUC. The ROC curve evaluates the correlation between sensitivity and specificity at different cut-points, which allows better assessment of the accuracy of the classification algorithm. Figure 8 shows lower AUC values for the images of SFC (0.72) and WC (0.86), while the highest value is for the images of PWC (0.95). These results indicate that ASD has the highest discriminatory power using PWC images. It is possible that the SVD helped to show the distribution of time–frequency components more consistently. Figure A1 in the Appendix B shows the differences in the distribution of the time–frequency components for one of the biomarkers in one of the subjects with ASD and a subject with NC before and after SVD.

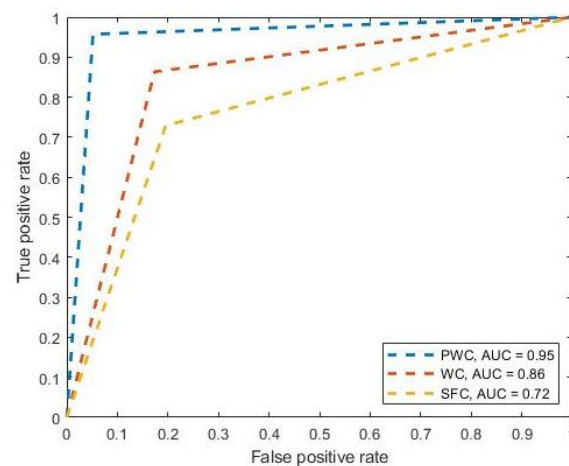


**Figure 8.** ROC curve and AUC of 3L-CNN using SFC, WC and PWC images.

#### 4.4.2. Evaluation of PWC-Based ASD Classification Using Testing/Unseen Images

The 10-fold CV method basically pools samples from all individuals and then separates them into 10-folds. The risk of bias in this strategy is due to inclusion of samples from the same person in both the training and test data, so the network can easily recognize the test data. While this type of bias leads to excellent performance, it can also be misleading, as the same network may not produce the same results on unseen data. Moreover, as the results would be clinically unreliable, this method is not suitable for ASD diagnosis. To address this problem, we use 10-fold cross validation on 90% of the dataset, while the remaining 10% of the data are completely unseen during training and are used to assess the performance of the trained network.

The classification results are given in Figure 9, which shows the confusion matrix of the 3L-CNN in detecting the PWC test images. From this confusion matrix, 525 ASD and 542 NC PWC images were correctly predicted by the model, while 36 ASD and 41 NC images were incorrectly predicted. Accordingly, these results yielded an overall accuracy, sensitivity and specificity of 93.3%, 93.6% and 93.0%, respectively, for ASD classification based on the test dataset. The results of this experiment show that our

proposed classification framework based on PWC images and 3L-CNN is a robust and effective ASD classification model for completely unseen data.

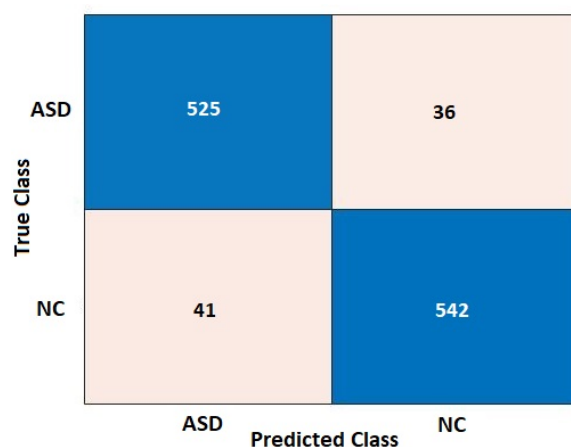


**Figure 9.** Confusion matrix for classification of PWC images of ASD and NC using the testing dataset.

#### 4.5. Comparison with Related Works

In recent years, several attempts have been made to develop computer-assisted diagnosis of ASD patients. In general, these studies have focused on rs-fMRI and related FC features with classification using classical ML techniques. The application of FC image-based deep learning algorithms for ASD diagnosis has recently shifted the focus of research, including in our work. To demonstrate the feasibility of our proposed framework, Table 5 compares the performance of existing models in ASD classification using the ABIDE dataset.

Good classification accuracies for the diagnosis of ASD based on SFC images have been obtained in previous studies [17,18] and are comparable to our results using SFC images with the proposed 3L-CNN model. However, these results are inferior to our results using dynamic FC images. Our proposed method using PWC images of ASD biological markers in CNN results in good accuracy of 95.2% based on 10-fold CV, e.g., 25.2%, 25% and 18.8% higher, respectively, than the methods proposed in [16–18]. On the other hand, our results outperform those of Wang et al. [22] by 2%. Accordingly, the dynamic FC features using PWC images play an important role in developing ASD classification performance compared to static FC features, which have a relatively small impact on ASD detection. Furthermore, the ASD biomarkers identified in our study can be utilized individually for ASD diagnosis. In conclusion, the PWC-based approach proposed in this study can help physicians with automatic and accurate detection of ASD in patients.

**Table 5.** Benchmarking with existing ASD classification methods using ABIDE dataset.

No.	References	Sample Size	FC Patterns	AI Algorithms	Accuracy	
1	Chen (2016) [19]	368	Dynamic	SVM	10-fold CV	79.2%
2	Bernas (2018) [20]	29	Dynamic	SVM	10-fold CV	86.7%
3	Heinsfeld (2018) [16]	1035	Static	DNN	10-fold CV	70.0%
4	Wang (2019) [22]	1054	Static	DNN	10-fold CV	93.2%
5	Sherkatghanad (2020) [17]	1035	Static	CNN	10-fold CV	70.2%
6	Huang (2020) [18]	1035	Static	DBN	10-fold CV	76.4%
7	Ma (2021) [21]	90	Dynamic	SVM	10-fold CV	78.9%
8	Subah (2021) [23]	866	Static	DNN	5-fold CV	87.9%
9	Our method	1035	Dynamic	CNN	10-fold CV	95.2%

## 5. Conclusions and Future Works

In this paper, an ASD classification framework comprising principal wavelet coherence (PWC) and a 3L-CNN is developed and thoroughly evaluated. In essence, PWC connectivity provides the neuronal biomarkers that are input to the 3L-CNN, which extracts and classifies features. The advantage of PWC to represent dynamic connectivity lies in the fact that it provides both time and frequency domain features that carry critical characteristic for discriminating ASD from NC subjects. Further, PWC is fundamentally the most discriminative feature of WC for ASD classification, as determined by a three-stage process: First, by ANOVA-SVM, providing 212 FCs, which were further distilled using correlation analysis between WCF and SRS scores, resulting in 11 FC. Lastly, application of SVD on the 11 FCs extracted the first principal subspace that sensed the maximal orientation energy of the PWC images. In other words, the input images of the 3L-CNN carry the most significant time–frequency information of the PWC and can be used as the biomarker for diagnosis of ASD. Evaluation of the proposed framework was conducted using the full ABIDE dataset, which includes 1035 individuals. PWC + 3LCNN achieved classification with the highest accuracy of 95.2% with a low error rate (4.8%). Comparison with state-of-the-art ASD classification models show the PWC method performs better than recently developed approaches.

Although PWC is promising for using fMRI features for ASD subtype diagnosis, it still has space for improvement. Furthermore, there is evidence that ASD and ADHD have overlapping symptoms, such as social withdrawal and communication difficulties [25,49]. ADHD is defined by a chronic pattern of inattention and/or hyperactivity and impulsivity that interferes with development. The overlap of symptoms in different brain disorders makes clinical diagnosis challenging, and classification models with multiple classes are needed for future studies of neurodevelopmental disorders. Future research on PWC images using CNN models could lead to a method for diagnosing ASD individuals using rs-fMRI data. To improve performance in multi-class classification, the use of different brain atlases, such as Craddock (CC200, CC400), that extract more information from the BOLD signals could be considered. Moreover, PWC images can also be trained and tested on other CNN architectures such as residual or inception blocks to achieve better classification of ASD subtypes. In addition, the proposed technique sheds light on computer-aided diagnosis of other psychological problems such as depression, schizophrenia and early Alzheimer's disease.

**Author Contributions:** M.I.A.-H. conducted the research and investigation process, finalised the methodology, proposed the algorithm and results analysis, and completed the manuscript writing. N.Y. formulated the research objective, provided supervision, validated the results and methodology, revised the manuscript and managed the funding of the project. I.F. provided some valuable suggestions and supervised the project. M.S.A.-Q. and A.A.-E. were involved in writing, reviewing and editing the final manuscript. All authors read and agreed to the published version of the manuscript.

**Funding:** This research is supported by two research grants: (1) The Ministry of Education of Malaysia under the Higher Institutional Centre of Excellence (HICoE) Scheme awarded to the Centre for Intelligent Signal and Imaging Research (CISIR); and (2) the Yayasan Universiti Teknologi PETRONAS under grant number YUTP-FRG 015LC0-292.

**Institutional Review Board Statement:** Not applicable.

**Informed Consent Statement:** Not applicable.

**Data Availability Statement:** Not applicable.

**Conflicts of Interest:** The authors declare no conflict of interest.

### Abbreviations

AAL	automated anatomical labeling
ABIDE	Autism Brain Image Data Exchange
ANOVA-SVM	analysis of variance-support vector machine
BOLD	blood oxygen level-dependent
DFC	dynamic functional connectivity
SFC	static functional connectivity
SVD	singular value decomposition
PCC	Pearson correlation coefficients
PWC	principal wavelet coherence
WC	wavelet coherence
WCF	wavelet coherence fluctuations
3L-CNN	three-layer convolutional neural network

### Appendix A

**Table A1.** Summary of previous AI algorithms in ASD classification using ABIDE rs-fMRI data.

No.	References	Sample Size	FC Patterns	FC Selection	AI Algorithms		Accuracy
1	Chen (2016) [19]	368	Dynamic	F-score	SVM	10-fold CV	79.2%
2	Heinsfeld (2018) [16]	1035	Static	—	DNN	10-fold CV	70.0%
3	Bernas (2018) [20]	29	Dynamic	—	SVM	10-fold CV	86.7%
4	Wang (2019) [22]	1054	Static	SVM-RFE	DNN	10-fold CV	93.2%
5	Sherkatghanad (2020) [17]	1035	Static	—	CNN	10-fold CV	70.2%
6	Huang (2020) [18]	1035	Static	Filter	DBN	10-fold CV	76.1%
7	Ma (2021) [21]	90	Dynamic	PCA	SVM	10-fold CV	78.9%
8	Subah (2021) [23]	866	Static	—	DNN	5-fold CV	87.9%

**Table A2.** Brain node connections with more than four significant positive or negative WCF correlations with SRS scores. The number in brackets is the *p*-value, which has a threshold at 95% confidence level, and the bold values are the *p*-values that exceed 0.05.

#	1st Node	Link	2nd Node	SRS_TOT	SRS_AWA	SRS_COG	SRS_COM	SRS_MOT	SRS_MAN	
Negative	1	Rolandic_Oper_L (ROL.L)	⇔	Rolandic_Oper_R (ROL.R)	−0.4 (0.02)	−0.4 (0.04)	−0.4 (0.02)	−0.4 (0.02)	−0.3 (0.09)	−0.4 (0.05)
	2	Frontal_Mid_R (MFG.R)	⇔	Hippocampus_R (HIP.R)	−0.5 (0.01)	−0.3 (0.12)	−0.4 (0.04)	−0.5 (0.01)	−0.5 (0.00)	−0.4 (0.02)
	3	Frontal_Sup_Medial_R (SFGmed.R)	⇔	Calcarine_L (CAL.L)	−0.4 (0.02)	−0.3 (0.14)	−0.4 (0.05)	−0.4 (0.04)	−0.4 (0.02)	−0.4 (0.04)
	4	Frontal_Sup_L (SFGdor.L)	⇔	Parietal_Sup_L (SPG.L)	−0.5 (0.01)	−0.5 (0.01)	−0.3 (0.15)	−0.5 (0.01)	−0.4 (0.01)	−0.3 (0.08)
	5	Olfactory_L (OLE.L)	⇔	SupraMarginal_R (SMG.R)	−0.5 (0.00)	−0.4 (0.05)	−0.5 (0.01)	−0.5 (0.00)	−0.4 (0.03)	−0.4 (0.02)
	6	Occipital_Sup_R (SOG.R)	⇔	Angular_L (ANG.L)	−0.4 (0.04)	−0.3 (0.14)	−0.4 (0.02)	−0.4 (0.06)	−0.3 (0.18)	−0.3 (0.13)
Positive	7	Postcentral_R (PoCG.R)	⇔	Parietal_Sup_R (SPG.R)	0.4 (0.05)	0.2 (0.33)	0.3 (0.09)	0.4 (0.05)	0.4 (0.05)	0.4 (0.04)
	8	Frontal_Sup_Orb_R (ORBsup.R)	⇔	Precuneus_L (PCUN.L)	0.4 (0.02)	0.1 (0.51)	0.4 (0.05)	0.4 (0.03)	0.4 (0.03)	0.4 (0.02)
	9	Angular_R (ANG.R)	⇔	Precuneus_R (PCUN.R)	0.5 (0.00)	0.3 (0.11)	0.4 (0.02)	0.6 (0.00)	0.4 (0.02)	0.5 (0.00)
	10	Thalamus_R (THA.R)	⇔	Temporal_Sup_R (STG.R)	0.5 (0.00)	0.5 (0.01)	0.4 (0.03)	0.5 (0.00)	0.5 (0.01)	0.4 (0.04)
	11	Angular_R (ANG.R)	⇔	Temporal_Pole_Mid_L (TPomid.L)	0.5 (0.01)	0.3 (0.09)	0.5 (0.00)	0.4 (0.02)	0.3 (0.11)	0.5 (0.01)

Bold values indicate insignificant correlation.

### Appendix B

**Table A3.** Classification performance of 3L-CNN using SFC images. The CNNs are evaluated based on the accuracy, sensitivity and specificity of 10-fold CV at different convolutional filter sizes (F.size), batch sizes (B.size) and optimization algorithms. Accordingly, the CNN achieved high scores based on F.size 7 × 7, B.size = 8 and ADAM optimizer.

B.Size	F.Size	Optimizer								
		ADAM			SGDM			Rmsprop		
		AccU	SenS	SpeC	AccU	SenS	SpeC	AccU	SenS	SpeC
8	7 × 7	72.3	72.4	73.2	71.5	75.5	67.6	66.2	66.9	65.5
	5 × 5	71.0	73.9	69.1	68.1	71.1	64.0	64.1	58.5	69.6
	3 × 3	70.0	69.6	70.5	67.7	68.3	67.1	65.6	64.6	66.6

Table A3. Cont.

B.Size	F.Size	Optimizer								
		ADAM			SGDM			Rmsprop		
		AccU	SenS	SpeC	AccU	SenS	SpeC	AccU	SenS	SpeC
16	7 × 7	70.8	69.7	71.9	59.9	60.2	59.5	54.3	55.0	53.6
	5 × 5	70.5	67.8	73.2	65.1	68.0	62.1	54.3	51.4	57.2
	3 × 3	68.0	81.8	54.2	66.8	73.7	59.9	62.0	60.5	63.3
24	7 × 7	69.9	74.7	65.1	64.1	56.0	57.7	58.2	57.2	60.0
	5 × 5	70.4	73.3	67.0	61.1	71.2	61.1	57.1	51.3	62.5
	3 × 3	61.0	63.0	60.0	63.6	70.4	56.9	58.1	55.1	61.1
32	7 × 7	71.9	78.6	65.2	57.7	65.8	49.6	52.3	58.0	46.7
	5 × 5	71.6	75.1	68.2	60.7	65.3	56.0	59.1	56.6	61.6
	3 × 3	67.4	66.6	68.3	63.4	74.7	52.1	59.1	52.1	67.1

## Appendix C

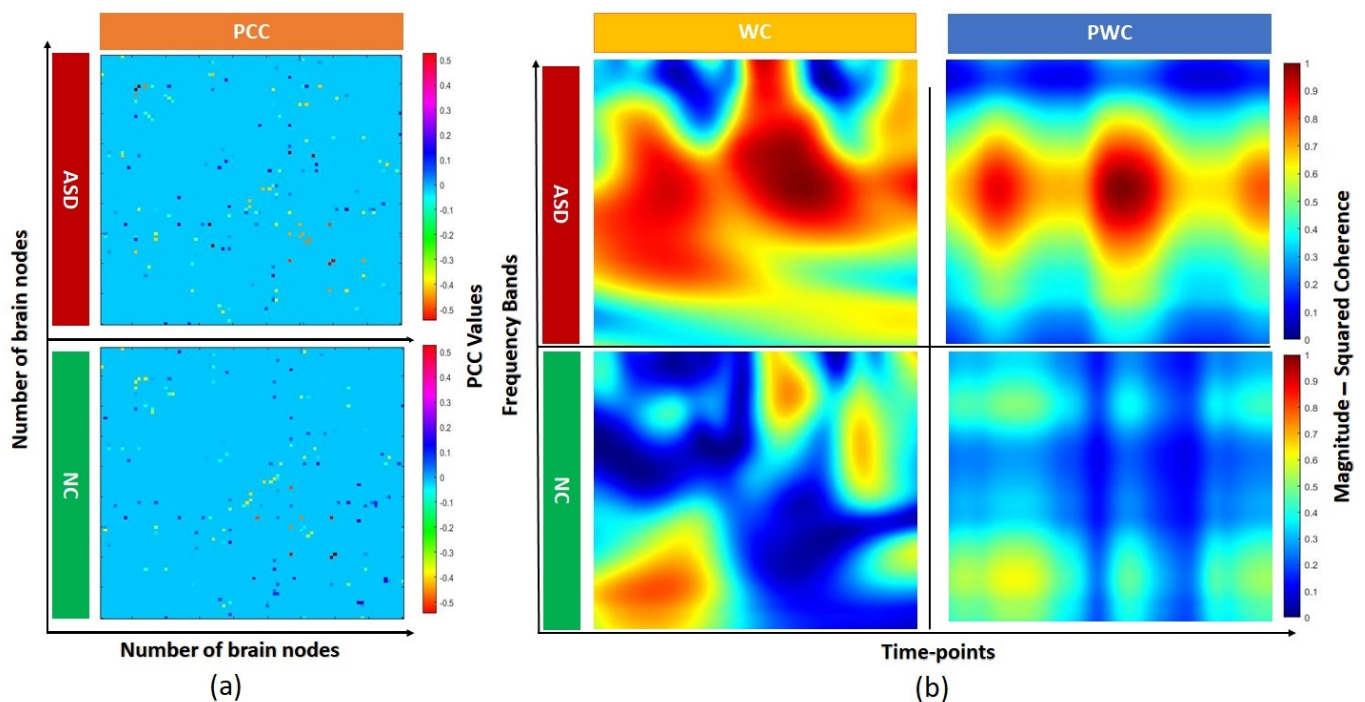


Figure A1. Samples of FC images for ASD and NC: (a) PCC, which is a type of SFC; and (b) WC and PWC, which is a type of DFC.

## References

1. Elsabbagh, M.; Divan, G.; Koh, Y.J.; Kim, Y.S.; Kauchali, S.; Marcín, C.; Montiel-Nava, C.; Patel, V.; Paula, C.S.; Wang, C.; et al. Global prevalence of autism and other pervasive developmental disorders. *Autism Res.* **2012**, *5*, 160–179. [[CrossRef](#)] [[PubMed](#)]
2. Emerson, N.D.; Morrell, H.E.; Neece, C. Predictors of age of diagnosis for children with autism spectrum disorder: The role of a consistent source of medical care, race, and condition severity. *J. Autism Dev. Disord.* **2016**, *46*, 127–138. [[CrossRef](#)] [[PubMed](#)]
3. Sadiq, A.; Al-Hiyali, I.M.; Norashikin, Y.; Tong Boon, T.; Khan, D.M. Non-Oscillatory Connectivity Approach for Classification of Autism Spectrum Disorder Subtypes Using Resting-State fMRI. *IEEE Access* **2022**, *10*, 14049–14061 [[CrossRef](#)]
4. Hogan, A.L.; Hills, K.J.; Wall, C.A.; Will, E.A.; Roberts, J. Screening and Diagnosis of Autism Spectrum Disorder in Preschool-Aged Children. In *Psychoeducational Assessment of Preschool Children*; Routledge: London, UK, 2020; pp. 323–345.
5. Chandler, S.; Charman, T.; Baird, G.; Simonoff, E.; Loucas, T.; Meldrum, D.; Scott, M.; Pickles, A. Validation of the social communication questionnaire in a population cohort of children with autism spectrum disorders. *J. Am. Acad. Child Adolesc. Psychiatry* **2007**, *46*, 1324–1332. [[CrossRef](#)] [[PubMed](#)]

6. Charman, T.; Baird, G.; Simonoff, E.; Loucas, T.; Chandler, S.; Meldrum, D.; Pickles, A. Efficacy of three screening instruments in the identification of autistic-spectrum disorders. *Br. J. Psychiatry* **2007**, *191*, 554–559. [[CrossRef](#)]
7. Norris, M.; Lecavalier, L. Screening accuracy of level 2 autism spectrum disorder rating scales: A review of selected instruments. *Autism* **2010**, *14*, 263–284. [[CrossRef](#)]
8. Lord, C.; Risi, S.; Lambrecht, L.; Cook, E.H.; Leventhal, B.L.; DiLavore, P.C.; Pickles, A.; Rutter, M. The Autism Diagnostic Observation Schedule—Generic: A standard measure of social and communication deficits associated with the spectrum of autism. *J. Autism Dev. Disord.* **2000**, *30*, 205–223. [[CrossRef](#)]
9. Abi-Dargham, A.; Horga, G. The search for imaging biomarkers in psychiatric disorders. *Nat. Med.* **2016**, *22*, 1248–1255. [[CrossRef](#)]
10. Klöppel, S.; Abdulkadir, A.; Jack, C.R., Jr.; Koutsouleris, N.; Mourão-Miranda, J.; Vemuri, P. Diagnostic neuroimaging across diseases. *Neuroimage* **2012**, *61*, 457–463. [[CrossRef](#)]
11. Bowman, F.D. Brain imaging analysis. *Annu. Rev. Stat. Its Appl.* **2014**, *1*, 61–85. [[CrossRef](#)]
12. Farahani, F.V.; Karwowski, W.; Lighthall, N.R. Application of graph theory for identifying connectivity patterns in human brain networks: A systematic review. *Front. Neurosci.* **2019**, *13*, 585. [[CrossRef](#)] [[PubMed](#)]
13. Biswal, B.; Zerrin Yetkin, F.; Haughton, V.M.; Hyde, J.S. Functional connectivity in the motor cortex of resting human brain using echo-planar MRI. *Magn. Reson. Med.* **1995**, *34*, 537–541. [[CrossRef](#)] [[PubMed](#)]
14. Greicius, M.D.; Krasnow, B.; Reiss, A.L.; Menon, V. Functional connectivity in the resting brain: A network analysis of the default mode hypothesis. *Proc. Natl. Acad. Sci. USA* **2003**, *100*, 253–258. [[CrossRef](#)]
15. Di Martino, A.; Scheres, A.; Margulies, D.S.; Kelly, A.; Uddin, L.Q.; Shehzad, Z.; Biswal, B.; Walters, J.R.; Castellanos, F.X.; Milham, M.P. Functional connectivity of human striatum: A resting state fMRI study. *Cereb. Cortex* **2008**, *18*, 2735–2747. [[CrossRef](#)] [[PubMed](#)]
16. Heinsfeld, A.S.; Franco, A.R.; Craddock, R.C.; Buchweitz, A.; Meneguzzi, F. Identification of autism spectrum disorder using deep learning and the ABIDE dataset. *Neuroimage Clin.* **2018**, *17*, 16–23. [[CrossRef](#)] [[PubMed](#)]
17. Sherkatghanad, Z.; Akhondzadeh, M.; Salari, S.; Zomorodi-Moghadam, M.; Abdar, M.; Acharya, U.R.; Khosrowabadi, R.; Salari, V. Automated Detection of Autism Spectrum Disorder Using a Convolutional Neural Network. *Front. Neurosci.* **2020**, *13*, 1325. [[CrossRef](#)] [[PubMed](#)]
18. Huang, Z.A.; Zhu, Z.; Yau, C.H.; Tan, K.C. Identifying autism spectrum disorder from resting-state fMRI using deep belief network. *IEEE Trans. Neural Netw. Learn. Syst.* **2020**, *32*, 2847–2861. [[CrossRef](#)]
19. Chen, H.; Duan, X.; Liu, F.; Lu, F.; Ma, X.; Zhang, Y.; Uddin, L.Q.; Chen, H. Multivariate classification of autism spectrum disorder using frequency-specific resting-state functional connectivity—A multi-center study. *Prog. Neuro-Psychopharmacol. Biol. Psychiatry* **2016**, *64*, 1–9. [[CrossRef](#)]
20. Bernas, A.; Aldenkamp, A.P.; Zinger, S. Wavelet coherence-based classifier: A resting-state functional MRI study on neurodynamics in adolescents with high-functioning autism. *Comput. Methods Programs Biomed.* **2018**, *154*, 143–151. [[CrossRef](#)]
21. Ma, X.; Wang, X.H.; Li, L. Identifying individuals with autism spectrum disorder based on the principal components of whole-brain phase synchrony. *Neurosci. Lett.* **2021**, *742*, 135519. [[CrossRef](#)]
22. Wang, C.; Xiao, Z.; Wang, B.; Wu, J. Identification of autism based on SVM-RFE and stacked sparse auto-encoder. *IEEE Access* **2019**, *7*, 118030–118036. [[CrossRef](#)]
23. Subah, F.Z.; Deb, K.; Dhar, P.K.; Koshiha, T. A deep learning approach to predict autism spectrum disorder using multisite resting-state MRI. *Appl. Sci.* **2021**, *11*, 3636. [[CrossRef](#)]
24. Hutchison, R.M.; Womelsdorf, T.; Allen, E.A.; Bandettini, P.A.; Calhoun, V.D.; Corbetta, M.; Della Penna, S.; Duyn, J.H.; Glover, G.H.; Gonzalez-Castillo, J.; et al. Dynamic functional connectivity: Promise, issues, and interpretations. *Neuroimage* **2013**, *80*, 360–378. [[CrossRef](#)] [[PubMed](#)]
25. Du, Y.; Fu, Z.; Calhoun, V.D. Classification and prediction of brain disorders using functional connectivity: Promising but challenging. *Front. Neurosci.* **2018**, *12*, 525. [[CrossRef](#)] [[PubMed](#)]
26. Abu-Akel, A.; Bousman, C.; Skafidas, E.; Pantelis, C. Mind the prevalence rate: Overestimating the clinical utility of psychiatric diagnostic classifiers. *Psychol. Med.* **2018**, *48*, 1225–1227. [[CrossRef](#)]
27. Fusar-Poli, P.; Hijazi, Z.; Stahl, D.; Steyerberg, E.W. The science of prognosis in psychiatry: A review. *JAMA Psychiatry* **2018**, *75*, 1289–1297. [[CrossRef](#)]
28. Craddock, C.; Benhajali, Y.; Chu, C.; Chouinard, F.; Evans, A.; Jakab, A.; Khundrakpam, B.S.; Lewis, J.D.; Li, Q.; Milham, M.; et al. The neuro bureau preprocessing initiative: Open sharing of preprocessed neuroimaging data and derivatives. *Front. Neuroinformatics* **2013**, *7*, 27.
29. Tzourio-Mazoyer, N.; Landeau, B.; Papathanassiou, D.; Crivello, F.; Etard, O.; Delcroix, N.; Mazoyer, B.; Joliot, M. Automated anatomical labeling of activations in SPM using a macroscopic anatomical parcellation of the MNI MRI single-subject brain. *Neuroimage* **2002**, *15*, 273–289. [[CrossRef](#)]
30. Van Dijk, K.R.; Hedden, T.; Venkataraman, A.; Evans, K.C.; Lazar, S.W.; Buckner, R.L. Intrinsic functional connectivity as a tool for human connectomics: Theory, properties, and optimization. *J. Neurophysiol.* **2010**, *103*, 297–321. [[CrossRef](#)]
31. Kazemi, Y.; Houghten, S. A deep learning pipeline to classify different stages of Alzheimer’s disease from fMRI data. In Proceedings of the 2018 IEEE Conference on Computational Intelligence in Bioinformatics and Computational Biology (CIBCB), St. Louis, MO, USA, 30 May–2 June 2018; pp. 1–8.

32. Al-Hiyali, M.I.; Yahya, N.; Faye, I.; Hussein, A.F. Identification of Autism Subtypes Based on Wavelet Coherence of BOLD fMRI Signals Using Convolutional Neural Network. *Sensors* **2021**, *21*, 5256. [[CrossRef](#)]
33. Grinsted, A.; Moore, J.C.; Jevrejeva, S. Application of the cross wavelet transform and wavelet coherence to geophysical time series. *Nonlinear Process. Geophys.* **2004**, *11*, 561–566. [[CrossRef](#)]
34. Morabito, F.C.; Campolo, M.; Mammone, N.; Versaci, M.; Franceschetti, S.; Tagliavini, F.; Sofia, V.; Fatuzzo, D.; Gambardella, A.; Labate, A.; et al. Deep learning representation from electroencephalography of early-stage Creutzfeldt-Jakob disease and features for differentiation from rapidly progressive dementia. *Int. J. Neural Syst.* **2017**, *27*, 1650039. [[CrossRef](#)] [[PubMed](#)]
35. Torrence, C.; Compo, G.P. A practical guide to wavelet analysis. *Bull. Am. Meteorol. Soc.* **1998**, *79*, 61–78. [[CrossRef](#)]
36. Al-Hiyali, M.I.; Yahya, N.; Faye, I.; Khan, Z. Autism Spectrum Disorder Detection Based on Wavelet Transform of BOLD fMRI Signals using Pre-trained Convolution Neural Network. *Int. J. Integr. Eng.* **2021**, *13*, 49–56. [[CrossRef](#)]
37. Al-Hiyali, M.I.; Yahya, N.; Faye, I.; Khan, Z.; Laboratoire, K.A. Classification of BOLD fMRI signals using wavelet transform and transfer learning for detection of autism spectrum disorder. In Proceedings of the 2020 IEEE-EMBS Conference on Biomedical Engineering and Sciences (IECBES), Langkawi Island, Malaysia, 1–3 March 2021; pp. 94–98.
38. Tang, C.; Wei, Y.; Zhao, J.; Nie, J. The dynamic measurements of regional brain activity for resting-state fMRI: d-ALFF, d-fALFF and d-ReHo. In Proceedings of the International Conference on Medical Image Computing and Computer-Assisted Intervention, Granada, Spain, 16–20 September 2018; Springer: Cham, Switzerland, 2018; pp. 190–197.
39. Chen, H.; Nomi, J.S.; Uddin, L.Q.; Duan, X.; Chen, H. Intrinsic functional connectivity variance and state-specific under-connectivity in autism. *Hum. Brain Mapp.* **2017**, *38*, 5740–5755. [[CrossRef](#)]
40. Nunes, A.S.; Peatfield, N.; Vakorin, V.; Doesburg, S.M. Idiosyncratic organization of cortical networks in autism spectrum disorder. *Neuroimage* **2019**, *190*, 182–190. [[CrossRef](#)]
41. Washington, P.; Paskov, K.M.; Kalantarian, H.; Stockham, N.; Voss, C.; Kline, A.; Patnaik, R.; Chrisman, B.; Varma, M.; Tariq, Q.; et al. Feature Selection and Dimension Reduction of Social Autism Data. In *Biocomputing 2020*; World Scientific: Singapore, 2019; pp. 707–718. [[CrossRef](#)]
42. Al-Ezzi, A.; Kamel, N.; Al-shargabi, A.; Yahya, N.; Faye, I.; Al-Hiyali, M.I. SVD-Based Feature Extraction Technique for The Improvement of Effective Connectivity Detection. In Proceedings of the 2021 International Conference on Intelligent Cybernetics Technology & Applications (ICICyTA), Bandung, Indonesia, 1–2 December 2021; pp. 52–57.
43. Khan, Z.; Yahya, N.; Alsaih, K.; Al-Hiyali, M.I.; Meriaudeau, F. Recent Automatic Segmentation Algorithms of MRI Prostate Regions: A Review. *IEEE Access* **2021**, *9*, 97878–97905. [[CrossRef](#)]
44. Hassan, S.U.; Zahid, M.S.M.; Abdullah, T.A.; Husain, K. Classification of cardiac arrhythmia using a convolutional neural network and bi-directional long short-term memory. *Digit. Health* **2022**, *8*, 20552076221102766. [[CrossRef](#)]
45. Gibbard, C.R.; Ren, J.; Skuse, D.H.; Clayden, J.D.; Clark, C.A. Structural connectivity of the amygdala in young adults with autism spectrum disorder. *Hum. Brain Mapp.* **2018**, *39*, 1270–1282. [[CrossRef](#)]
46. Xu, Q.; Zuo, C.; Liao, S.; Long, Y.; Wang, Y. Abnormal development pattern of the amygdala and hippocampus from childhood to adulthood with autism. *J. Clin. Neurosci.* **2020**, *78*, 327–332. [[CrossRef](#)]
47. Wymbs, N.F.; Nebel, M.B.; Ewen, J.B.; Mostofsky, S.H. Altered inferior parietal functional connectivity is correlated with praxis and social skill performance in children with autism spectrum disorder. *Cereb. Cortex* **2021**, *31*, 2639–2652. [[CrossRef](#)] [[PubMed](#)]
48. Yahya, N.; Kamel, N.S.; Malik, A.S. Subspace-Based Technique for Speckle Noise Reduction in SAR Images. *IEEE Trans. Geosci. Remote Sens.* **2014**, *52*, 6257–6271. [[CrossRef](#)]
49. Taurines, R.; Schwenck, C.; Westerwald, E.; Sachse, M.; Siniatchkin, M.; Freitag, C. ADHD and autism: Differential diagnosis or overlapping traits? A selective review. *ADHD Atten. Deficit Hyperact. Disord.* **2012**, *4*, 115–139. [[CrossRef](#)] [[PubMed](#)]